Biomaterials Science

ROYAL SOCIETY OF CHEMISTRY

PAPER

View Article Online
View Journal | View Issue

Cite this: *Biomater. Sci.*, 2023, **11**, 1765

Histidine-based coordinative polymers for efficient intracellular protein delivery *via* enhanced protein binding, cellular uptake, and endosomal escape†

Changyuan Chen,[a] Peng Gao,[a] Hui Wang,[a] Yiyun Cheng *[b] and Jia Lv*[b]

Received 25th September 2022,
Accepted 13th December 2022

DOI: 10.1039/d2bm01541b

rsc.li/biomaterials-science

Polymers are one of the most promising protein delivery carriers; however, their applications are hindered by low delivery efficacy owing to their undesirable performance in protein binding, cellular uptake and endosomal escape. Here, we designed a series of histidine-based coordinative polymers for efficient intracellular protein delivery. Coordination of metal ions such as Ni^{2+}, Zn^{2+}, and Cu^{2+} with histidine residues on a polymer greatly improved its performance in protein binding, complex stability, cellular uptake and endosomal escape, therefore achieving highly improved protein delivery efficacy. Among the coordinative polymers, the Zn^{2+}-coordinated one exhibited the highest cellular uptake, while the Cu^{2+}-coordinated one exhibited the highest endosomal escape. The Ni^{2+}-coordinated polymer formed large-sized aggregates with cargo proteins and showed insufficient protein release after endocytosis. The results obtained in this study provided new insight into the development of coordinative polymer-based protein delivery systems.

1. Introduction

Protein therapeutics with high bioactivity and specificity show a promising prospect in disease treatment.[1] Since the advent of recombinant human insulin in the 1980s, protein drugs have revolutionized the pharmaceutical industry. Hundreds of protein therapeutics have been approved by the FDA for clinical use, and five of the top ten best-selling drugs were proteins last year.[2,3] Despite the progress, all of the marketed protein drugs function extracellularly due to their limited membrane permeability.[4] Developing efficient intracellular protein transfer carriers plays an important role in the development of cytosolic protein-related biotherapeutics and biotechnology.[5]

In the past few decades, carriers including cell-penetrating domains, lipids, inorganic nanoparticles, polymers, nanogels, metal–organic frameworks, exosomes, and recombinant virus mimics have been developed to transport proteins into living cells.[6–8] Among them, polymeric carriers have gained increasing attention owing to their promising features including controllable structures, good water solubility, and ease of fabrication and modification.[9–11] A conventional protein delivery strategy relies on ionic interactions between polymers and cargo proteins. However, this method is only suitable for proteins with certain charge properties, and the formed complexes are generally not stable and are easily disturbed under physiological conditions. To improve the stability of complexes, proteins were covalently conjugated with polymeric carriers.[12,13] Alternatively, negatively charged moieties were introduced into cargo proteins to enhance their binding affinity to cationic polymers *via* electrostatic interaction.[14,15] Besides, non-covalent molecular recognition motifs such as avidin/biotin and cyclodextrin/adamantane were also introduced into polymeric protein delivery systems to improve complex stability.[16] These strategies showed good prospects in cytosolic protein delivery, but are involved with complicated biological or chemical modifications, which may alter the bioactivity of cargo proteins. To address this concern, ligands such as guanidinium,[15,17,18] boronate,[19,20] metal chelates,[21,22] and catechol[23] with high protein binding affinity were introduced into cationic polymers to enhance complex stability *via* multiple non-covalent interactions, *i.e.*, salt bridge, nitrogen–boronate coordination, nitrogen–metal coordination, hydrogen bonding and hydrophobic interactions. Besides, amphiphilic polymers were constructed to encapsulate native proteins and form stable complexes *via* supramolecular self-assembly.[24–26] The complex stability was further improved *via* stimuli-respon-

[a]*South China Advanced Institute for Soft Matter Science and Technology, School of Molecular Science and Engineering, South China University of Technology, Guangzhou, 510640, China*
[b]*Shanghai Frontiers Science Center of Genome Editing and Cell Therapy, Shanghai Key Laboratory of Regulatory Biology, School of Life Sciences, East China Normal University, Shanghai, 200241, China. E-mail: yycheng@mail.ustc.edu.cn, jlv@bio.ecnu.edu.cn*

† Electronic supplementary information (ESI) available. See DOI: https://doi.org/10.1039/d2bm01541b

sive cross-linking among the polymers, by which efficient cytosolic protein delivery was achieved *in vivo*.[27] After endocytosis, entrapment of the complexes in the endosomal–lysosomal system is another major obstacle for the existing carriers.[28] To overcome this impediment, endosomolytic polymers, lipids, peptides, and surfactants were introduced to facilitate the endosomal escape process.[29–32] Although some achievements have been made, the rational design of materials with high efficacy for both protein binding and endosomal escape is still highly desired.

To achieve robust protein encapsulation, the carriers are proposed to have strong binding affinity to universal cargo proteins. Immobilized metal ion affinity chromatography (IMAC) is a widely used technique for protein binding and separation,[33] which is based on the coordinative and/or ionic interactions between immobilized metal chelates and proteins. Metal chelates such as Ni-nitrilotriacetic acid (Ni-NTA) have strong binding affinity to peptides, such as the well-known His-tag containing six histidine residues (His_6, $K_d < 10^{-7}$ M). Several carrier systems were constructed by incorporating Ni-chelates for His_6-tagged protein delivery.[13,34] Besides Ni^{2+}, transition metal ions such as Zn^{2+} and Cu^{2+} have high binding affinity to various amino acids, such as histidine, glutamic acid, aspartic acid, cysteine, and methionine.[35] Here, we developed a series of coordinative polymers based on the high binding affinity between the metal chelates and amino acids for intracellular protein delivery. Histidine proteins were modified with an amine-terminated generation 5 (G5) polyamidoamine (PAMAM) dendrimer, and further chelated with metal ions including Ni^{2+}, Zn^{2+}, and Cu^{2+} to obtain the coordinative polymers. In the delivery system, the polymeric scaffold containing the PAMAM dendrimer and histidine may promote endosomal escape *via* the "proton sponge effect",[36] and the prepared polymers are proposed to bind with cargo proteins and form stable complexes *via* a synergetic effect of coordination and ionic interactions. The incorporation of metal ions may also facilitate endocytosis and endosomal escape of the protein complexes owing to their increased binding affinity to phospholipids on cell membranes. After cell internalization, the cargo proteins could be released triggered by polyanions, proteins, and glutathione (GSH) to exert their bioactivity.[37,38]

2. Materials and methods

2.1. Materials

The amine-terminated G5 PAMAM dendrimer was ordered from Dendritech (USA). Dicyclohexylcarbodiimide, *N*-hydroxysuccinimide, and triethylamine were bought from Adamas Reagent (China). Boc-His (Trt)–OH was purchased from GL Biochem (China). Trifluoroacetic acid was bought from Meryer (China). $NiCl_2{\cdot}6H_2O$ and $CuCl_2{\cdot}2H_2O$ were ordered from Macklin (China). $ZnCl_2$ was bought from Merck (USA). Rhodamine B isothiocyanate (RB) was obtained from Yuanye Bio. (China). β-Galactosidase (β-Gal) was ordered from J&K Scientific (China). Lyso-Tracker red, β-Gal activity assay kits, and Hoechst 33342 were obtained from Beyotime (China). PULSin and TransExcellent (TransEx) were obtained from Polyplus Transfection (France) and Cenji Biotech. (China), respectively. A yellow fluorescent protein-tagged galectin 8 (Gal 8-YFP) plasmid was obtained as a gift from Prof. Felix Randow in the MRC Laboratory of Molecular Biology.

2.2. Synthesis and characterization of histidine-modified dendrimers

Boc-His (Trt)–OH, dicyclohexylcarbodiimide and *N*-hydroxysuccinimide were dissolved in anhydrous *N*,*N*-dimethyl formamide at a molar ratio of 1 : 1.2 : 1.3 and stirred for 6 hours to activate the carboxyl group. The G5 PAMAM dendrimer dissolved in anhydrous dimethyl sulfoxide was added to the above solution, followed by the addition of triethylamine. The molar ratio of triethylamine to Boc-His (Trt)–OH was 1.5 : 1, and the ratios of Boc–His(Trt)–OH to the dendrimer were 50 : 1, 80 : 1, 100 : 1 and 180 : 1, respectively. The solution mixtures were stirred at room temperature for 7 days and then dialyzed with dimethyl sulfoxide and freeze-dried. The products were dissolved in a mixture of dichloromethane and trifluoroacetic acid at a volume ratio of 1 : 4 and stirred at room temperature for 6 hours to remove the Boc and Trt moieties. The solvents were removed by rotary evaporation and the remaining crude products were intensively dialyzed against dimethyl sulfoxide and distilled water, and then freeze-dried to obtain the histidine-modified dendrimers. The average number of histidine ligands modified on each dendrimer was characterized by ^{1}H NMR spectroscopy (Avance 500, Bruker, Germany).

2.3. Preparation of coordinative polymers

The synthesized histidine-modified dendrimers were dissolved in methanol, followed by the addition of $CuCl_2$ at Cu^{2+} to histidine molar ratios of 0.5 : 1, 1 : 1, or 2 : 1, respectively. After stirring at 37 °C for 3 hours, methanol was removed to obtain Cu^{2+}-coordinated polymers. The Ni^{2+}- and Zn^{2+}-coordinated polymers were obtained using the same procedure. The coordinative polymers were characterized by ultraviolet-visible spectroscopy (UV-Vis, Cary 60, Agilent, USA) and X-ray photoelectron spectroscopy (XPS, EscaLab Xi$^+$, Thermo Fisher, USA).

2.4. Synthesis and characterization of RB-labeled polymers

The dendrimer modified with 80 histidine (G5-His 80) was mixed with RB at a molar ratio of 1 : 3 in deionized water and stirred at room temperature for 24 hours. The crude products were dialyzed with deionized water and lyophilized to obtain the RB-labeled polymer, then the polymer was dissolved in methanol and added with $CuCl_2$, $NiCl_2$, and $ZnCl_2$, respectively, at a molar ratio of 1 : 1 to obtain the RB-labeled coordinative polymers as described above. The spectra of the obtained polymers were characterized using a fluorescence spectrophotometer (F-320, Ex: 520 nm; Em: 570 nm–610 nm).

To investigate the release of metal ions from the coordinative polymers in the cytosol, the RB-labeled coordinative polymers were dissolved in deionized water and added to a cyto-

plasm mimic buffer containing BSA (0.5 mg mL^{-1}), heparin (0.5 mg mL^{-1}) and GSH (5 mM). After 30 minutes of incubation, the spectra of the polymers were recorded using a fluorescence spectrophotometer (Ex: 520 nm; Em: 570 nm–610 nm).

2.5. Synthesis and characterization of the RB-labeled protein

β-Gal was mixed with RB in PBS and stirred at 4 °C for 24 hours, followed by dialysis at 4 °C with deionized water and lyophilized to obtain β-Gal-RB as red powders. The obtained β-Gal-RB was stored at −20 °C.

2.6. Preparation and characterization of polymer/protein complexes

The coordinative polymers were mixed with cargo proteins at weight ratios ranging from 0.8 : 1 to 2 : 1 in 50 μL deionized H_2O, PBS, or serum-free Dulbecco's modified Eagle's medium (DMEM). The mixtures were incubated at room temperature for 30 minutes, and then diluted with deionized water, PBS, and DMEM, respectively. The size and zeta potential of the complexes were analyzed by dynamic light scattering (DLS), the morphologies of the complexes were observed by transmission electron microscopy (TEM), and the secondary structures of the cargo proteins in the complexes were determined by circular dichroism spectroscopy. The protein binding capability of carriers was analyzed by agarose gel electrophoresis and sodium dodecyl sulfate–polyacrylamide gel electrophoresis (SDS-PAGE). Briefly, the complexes were centrifuged at a speed of 12 000 rpm for 20 minutes, and the free proteins in the supernatant were collected and mixed with the same volume of 5% glycerol. 15 μL of the mixture was loaded on the agarose gel and run at 80 V for 15 minutes. The proteins on the gels were stained with Coomassie Brilliant Blue G-250 and visualized using a gel image system (GelView 5000ProII, Biolight Biotechnology, China). The protein binding ratios were quantitively evaluated using image J software based on the gray intensity of protein bands. For SDS-PAGE, after centrifugation, the proteins in the precipitates were dissolved in 1× protein loading buffer containing 2-mercaptoethanol and heated at 100 °C for 10 min. After that, the proteins were loaded on the sodium dodecyl sulfate–polyacrylamide gel and run at 90 V for 80 min. The proteins on the gels were stained with Coomassie Brilliant Blue G-250 and visualized using a gel image system.

2.7. Cell culture and intracellular protein delivery

HeLa (human cervical cancer cells), 143B (human osteosarcoma cells), CHO (Chinese hamster ovary cells), and NIH3T3 (mouse embryo fibroblast cells) were obtained from ATCC. iWAT (mouse inguinal white adipocyte cells) and BAT (mouse brown adipose tissue cells) were gifts from Prof. Xinran Ma (East China Normal University). All the cells were cultured in DMEM (Gibco) supplemented with 10% (v/v) fetal bovine serum (FBS, Gemini), and 100 units per mL penicillin sulfate and streptomycin. The cells were seeded in 48-well plates or confocal cell culture dishes and incubated overnight until reaching a confluence of 80%–90%. The cells were treated with the polymer/protein complexes prepared in serum-free DMEM described above for 2–6 hours, and then washed thrice with PBS. For EGFP, after further washing with trypan blue (0.04%) to quench the extracellular fluorescent proteins, the cells were observed by laser scanning confocal microscopy (LSM 880, Carl Zeiss, Germany). The fluorescence intensity of the treated cells was quantitively analyzed by flow cytometry (FACS Verse, BD, USA). For β-Gal, the enzymatic activities of the cargo proteins in the treated cells were qualitatively and quantitatively tested using an *in situ* β-Gal staining kit and a β-Gal assay kit, respectively. The enzymatic activity of blank cell lysates containing the same dose of β-Gal was determined as 100%.

For the endocytosis pathway assay, HeLa cells were pretreated with cytochalasin D (inhibitor of micropinocytosis, 10 μM), genistein (inhibitor of the caveolin-involved pathway, 700 μM), methyl-β-cyclodextrin (MβCD, inhibitor of lipid rafts, 10 mM), and chlorpromazine (inhibitor of the clathrin-involved pathway, 20 μM) for 1 hour, respectively, before incubation with the complexes. The cells were preincubated at 4 °C for 1 hour and then incubated with the complexes at 4 °C and were tested to investigate the energy-dependence of internalization processes. The fluorescence intensity of the complex-treated cells at 37 °C without inhibitor treatment was set as 100%.

2.8. Endosomal disruption assay

Packaging plasmid pCMV-VSV-G and plasmid Gal 8-YFP were delivered into HEK 293 cells using Lipofectamine 2000 to produce pseudotyped lentiviral particles. HeLa cells were transfected with the produced lentiviral particles, followed by selection with puromycin. HeLa cells stably expressing Gal 8-YFP (Gal 8-YFP-HeLa) were obtained by single cloning amplification *via* limited dilution in a puromycin-containing medium.

For the endosomal disruption assay, Gal 8-YFP-HeLa cells were seeded in confocal cell culture dishes and incubated overnight until reaching a confluence of 80%–90%. The cells were incubated with the polymer/protein complexes for 2–6 hours, then washed with PBS three times and observed by laser scanning confocal microscopy. Hoechst 33342 (1×) was used to stain the nuclei at 37 °C for 1 hour. The endosomal disruption was quantified by counting the yellow fluorescent dots in the treated cells.

2.9. Cell viability assay

HeLa cells seeded in 96-well plates were treated with the polymers at different concentrations until reaching 80% confluence. After 6 hours of incubation, the cells were refreshed with DMEM containing 10% FBS, and further incubated for 18 hours. The viabilities of the treated cells were tested using a standardized 3-(4,5-dimethyl-2-thiazolyl)-2,5-diphenyl-2-*H*-tetrazolium bromide (MTT) assay.

2.10. Data analysis

The data were shown as mean ± SD (n = 3 for the protein delivery experiments, and n = 5 for the MTT assay). The significant differences between the two groups were analyzed by a one-

tailed Student's *t*-test. $^{N.S.}p \geq 0.05$, $^{*}p < 0.05$, $^{**}p < 0.01$ and $^{***}p < 0.001$.

3. Results and discussion

3.1. Preparation and characterization of the coordinative polymers

The histidine-modified G5 PAMAM dendrimer (G5-His) was synthesized by a facile reaction as shown in Fig. 1a. An average number of 80 histidine ligands were modified on each dendrimer as characterized by ^{1}H NMR (Fig. 1b). The obtained polymer was coordinated with Cu^{2+}, Ni^{2+}, and Zn^{2+} at a metal ion/histidine molar ratio of 1 : 1 (Fig. 1a) to obtain the coordinative polymers G5-His 80 Cu, G5-His 80 Ni, and G5-His 80 Zn, respectively. The coordination between metal ions and His ligands was analyzed by UV-Vis spectroscopy. As shown in Fig. 1c, the absorption peaks of Cu^{2+} in $CuCl_2$ and the His moiety in G5-His 80 were observed at 765 nm and 268 nm, respectively. After coordination, the absorption peak of Cu^{2+} was shifted to about 575 nm, and the band of His moieties showed a bathochromic shift, indicating coordination interactions between Cu^{2+} and His moieties. Similar phenomena were observed for G5-His 80 Ni (Fig. S1†) and G5-His 80 Zn (Fig. S2†). The coordination between metal ions and His ligands was further investigated by XPS. As shown in Fig. 1d, the signals of O, N, and C from G5-His 80 and those of Cu, Ni, and Zn ions were observed in the XPS spectrum of G5-His 80 Cu, G5-His 80 Ni and G5-His 80 Zn, respectively. The N 1s spectrum of G5-His 80 was deconvoluted into four peaks at 398.36 eV, 399.1 eV, 399.83 eV, and 400.67 eV, which were assigned to C=N, C–NH–C, N–C=O, and C–NH_3^+, respectively (Fig. 1e). After Cu^{2+} coordination, the N 1s peaks of C=N, C–NH–C, and C–NH_3^+ were shifted to higher binding energies

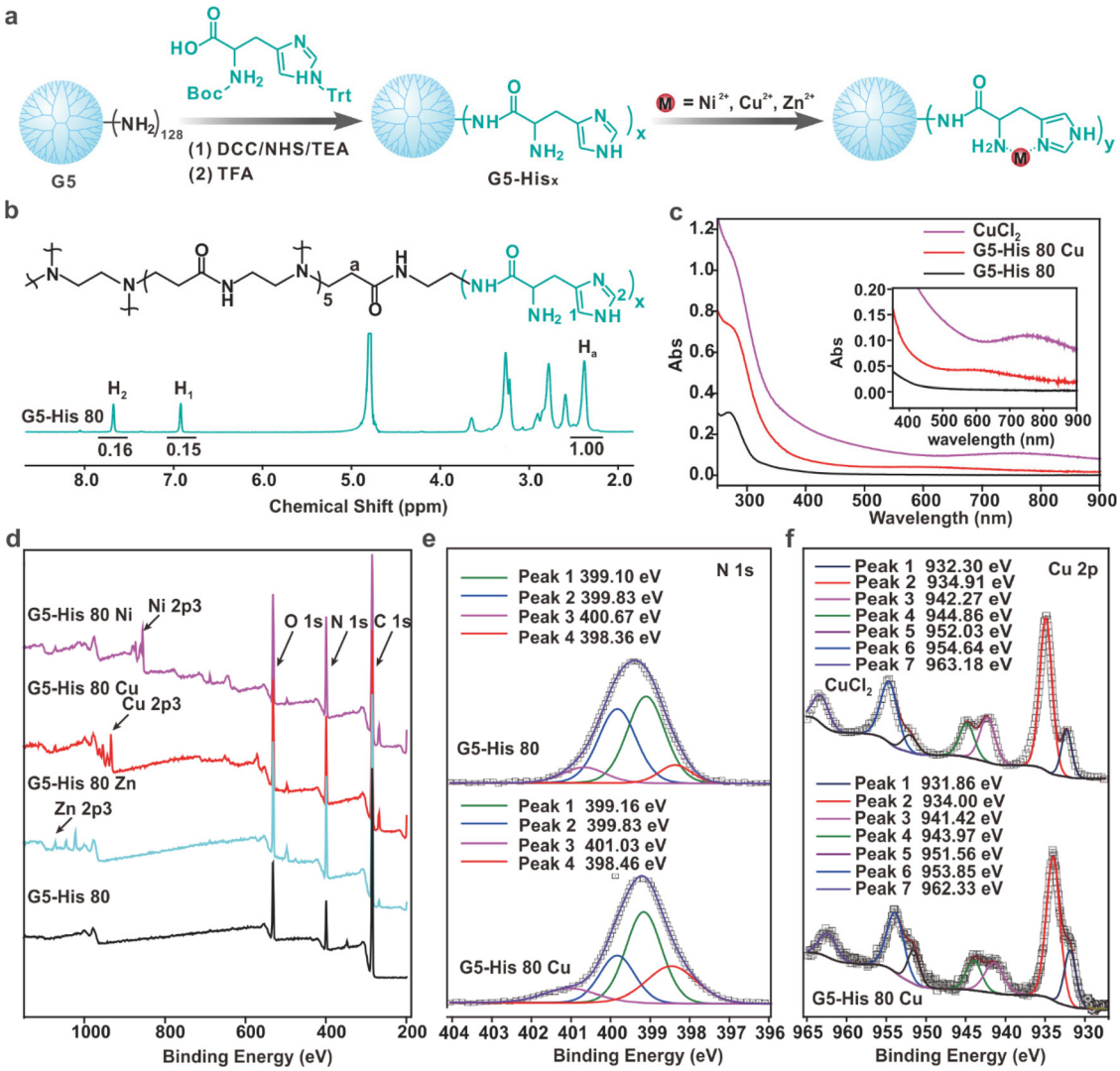

Fig. 1 Synthesis and characterization of the coordinative polymers. (a) Preparation of the coordinative polymers. (b) ^{1}H NMR spectrum of G5-His 80 in D_2O. (c) UV-Vis spectra of $CuCl_2$, G5-His 80 Cu, and G5-His 80 in aqueous solution. (d) XPS spectra of G5-His 80 Ni, G5-His 80 Cu, G5-His 80 Zn, and G5-His 80. (e) Magnified XPS N 1s spectra of G5-His 80 and G5-His 80 Cu. (f) Magnified XPS Cu 2p spectra of $CuCl_2$ and G5-His 80 Cu.

(Fig. 1e), and all the peaks of Cu 2p were shifted to lower binding energies (Fig. 1f), indicating the donation of electrons from imidazole and amine of His moieties to Cu^{2+}. Similar phenomena were observed in the XPS spectra of G5-His 80 Ni (Fig. S3†) and G5-His 80 Zn (Fig. S4†), suggesting the successful coordination between metal ions and G5-His 80.

3.2. Intracellular protein delivery by coordinative polymers

The intracellular protein delivery efficacy of the obtained coordinative polymers was tested using an enhanced green fluorescent protein (EGFP) as the model protein. As shown in Fig. 2a and b, coordination of metal ions significantly improved the EGFP delivery efficacy of G5-His 80 on HeLa cells. Among the coordinative polymers, G5-His 80 Cu showed the highest delivery efficacy, followed by G5-His 80 Zn, and both polymers were superior to commercial protein delivery reagents TransEx and PULSin. G5-His 80 Ni also delivered the EGFP into the treated cells; however, the delivered cargo proteins were mainly distributed as large spots in the treated cells and not well-dispersed in the cytosol with the increasing culture time (Fig. 2b and S5†). G5-His 80 without metal ion coordination showed negligible cytosolic protein delivery. The coordinative polymers exhibited low cytotoxicity at the tested concentrations (Fig. S6†).

3.3. Mechanism of coordinative polymers in cytosolic protein delivery

We then investigated the reason why the coordinative polymers, especially G5-His 80 Cu, exhibited superior delivery efficacy toward G5-His 80. We first tested the protein binding efficacy and the complex stability of the obtained polymers using an agarose gel electrophoresis assay. As shown in Fig. 2c and d, all the polymers including G5-His 80 and the coordinative polymers bound to more than 85% of the fed EGFP in aqueous solution, and the complex changed the secondary structure of the cargo protein (Fig. S7†). However, when diluted with PBS and DMEM, G5-His 80 released most of the bound EGFPs (57% for PBS and 86% for DMEM). The complexes formed by the coordinated polymers and EGFP were relatively stable and most of the cargo proteins remained in the complexes. This result indicates the beneficial effect of metal ions in enhancing the stability of polymer/protein complexes. Besides the EGFP, the coordinated polymers showed high binding affinity to cargo proteins with different molecular

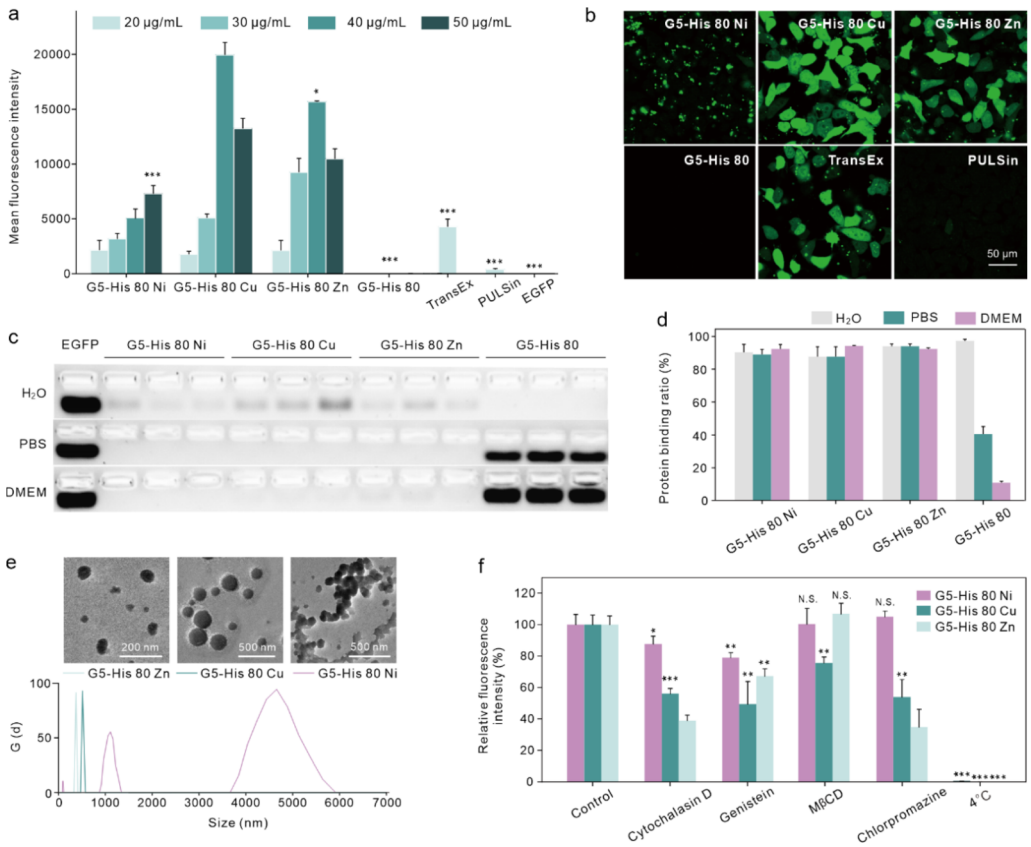

Fig. 2 Coordinative polymers for intracellular EGFP delivery. Flow cytometry analysis (a) and confocal images (b) of HeLa cells treated with polymer/EGFP complexes for 6 h. The concentration of EGFP was 25 μg mL^{-1}. Protein encapsulation of the polymers analysed *via* agarose gel electrophoresis (c) and quantitatively analysed according to the electrophoresis results (d). (e) Size distribution and TEM images of the G5-His 80 Ni/EGFP, G5-His 80 Ni/EGFP, and G5-His 80 Zn/EGFP complexes. The weight ratio of the coordinative polymer to the EGFP was 1.6 : 1. (f) Endocytosis pathways of coordinative polymer/EGFP complexes.

weights and charge properties such as bovine serum albumin (69.3 kDa, pI 4.7), horseradish peroxidase (40.0 kDa, pI 7.2), and trypsin (24 kDa, pI 10.5) (Fig. S8†). DLS results revealed that all the polymer/protein complexes were positively charged. The sizes of G5-His 80 Cu/EGFP and G5-His 80 Zn/EGFP complexes were around 500 nm and 100 nm, respectively. G5-His 80 Ni/EGFP, however, had a large size of around 4–6 μm (Fig. 2e), which was much larger than the polymer/protein complexes reported before.[39,40] To figure out how cells take up such big particles, the internalization process of G5-His 80 Ni/EGFP complexes was monitored by live cell imaging (Movie S1†). It was interesting to observe that HeLa cells tore off nanocomplexes from big particles and swallowed them bit by bit. TEM images revealed that although micron-sized aggregates were observed for G5-His 80 Ni/EGFP complexes, the aggregates were mainly formed by stacking of polymer/protein complexes smaller than 100 nm (Fig. 2e), and cells could tear off these submicron complexes from the aggregates for endocytosis. An endocytosis mechanism study revealed that internalization of the coordinative polymer/EGFP complexes by HeLa cells was energy-dependent and involved multiple pathways (Fig. 2f). In particular, G5-His 80 Ni/EGFP complexes were internalized *via* micropinocytosis and the caveolin-associated pathway. G5-His 80 Zn/EGFP complexes were internalized by micropinocytosis and the caveolin- and clathrin-associated pathways. The endocytosis of G5-His 80 Cu/EGFP complexes was inhibited by cytochalasin D, genistein, MβCD, and chlorpromazine, involving micropinocytosis-, clathrin-, lipid raft-, and caveolin-related pathways, respectively.

To further compare the cellular uptake of the polymers, G5-His 80 was labelled with a red fluorescent dye RB before coordination with the metal ions. Coordination of Cu^{2+} and Ni^{2+} significantly decreased the fluorescence of G5-His 80-RB (Fig. 3a), while the quenched fluorescence was fully recovered in a cytoplasm mimetic buffer containing 5 mM GSH (Fig. 3b),[38,41] indicating efficient metal ion release from the coordinative polymers in the cytoplasm. The RB-labelled polymers were incubated with HeLa cells for 6 h and the cellular uptake of the polymers was quantitatively analyzed by flow cytometry. As shown in Fig. 3c, metal ion coordination signifi-

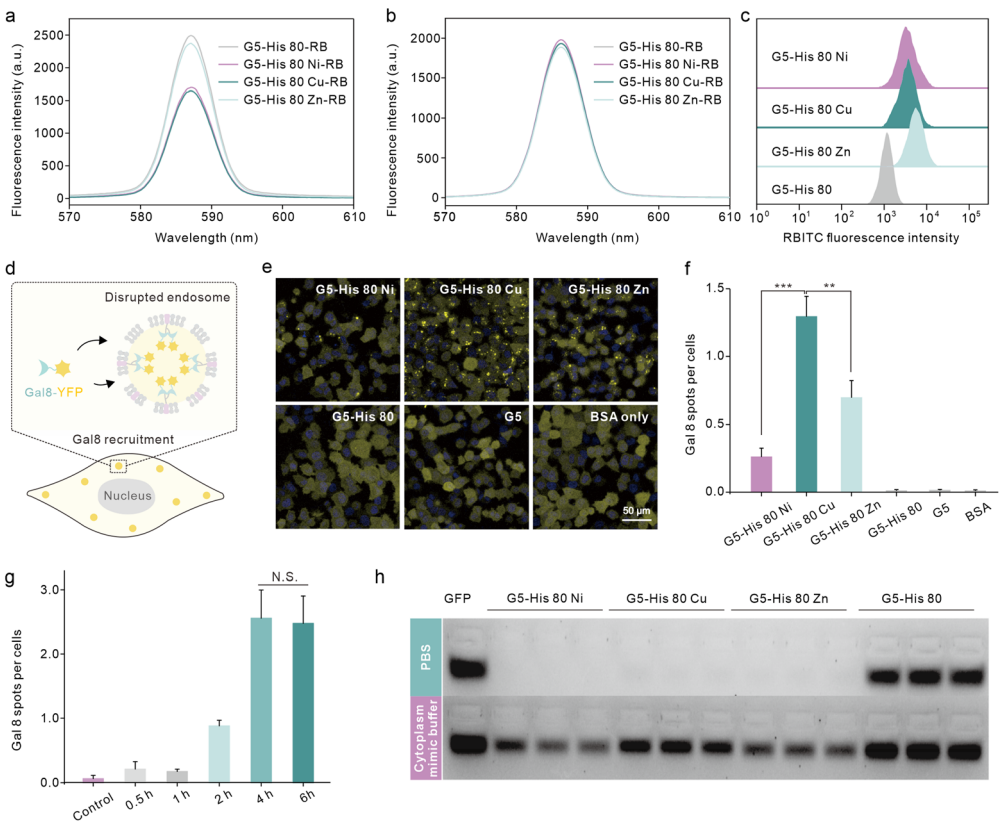

Fig. 3 Cellular uptake, endosomal escape and protein release behaviors of the coordinative polymers. Fluorescence spectra of G5-His 80-RB, G5-His 80 Ni-RB, G5-His 80 Cu-RB, and G5-His 80 Zn-RB in aqueous solution before (a) and after (b) the addition of glutathione (5 mM). (c) Cellular uptake of RB-labeled polymers on HeLa cells after 6 h treatment. The concentration of polymers was 40 μg mL^{-1}. (d) Schematic illustration of Gal8 recruitment into disrupted endosomes. (e) Fluorescence images of Gal8-YFP-HeLa cells after 6-hour treatment with the polymer/BSA complexes. (f) Average fluorescent spots per cell in (e) analyzed using image J. The concentrations of the polymer and the EGFP were 40 μg mL^{-1}, and 25 μg mL^{-1}, respectively. (g) Average fluorescent spots of Gal8-YFP-HeLa cells treated with G5-His 80 Cu/BSA complexes for 0.5–6 hours. (h) EGFP release from the coordinative polymers in the cytoplasm mimic buffer (GSH 5 mM, BSA 0.5 mg mL^{-1}, heparin 0.5 mg mL^{-1}) analyzed by agarose gel electrophoresis. The weight ratio of the polymers to the EGFP was 1.6 : 1.

cantly enhanced the uptake of G5-His 80 by HeLa cells, and G5-His 80 Zn showed the highest cellular uptake among the polymers.

Endo–lysosomal entrapment after endocytosis is a challenging issue that hinders efficient cytosolic protein delivery.[28] We hence tested the endosomal escape ability of the complexes in Gal8-YFP-HeLa. Gal8 is a β-galactoside-binding lectin dispersed in the cytosol and has high binding affinity to galactosides distributed in the inner leaflet of endosomal membranes. Gal8-YFP could be localized on damaged endosomes *via* molecular recognition (Fig. 3d) and the endosomal disruptions in the treated cells could be directly observed according to YFP spots.[42] As shown in Fig. 3e, obvious Gal8-YFP recruitment was observed in cells treated with the coordinative polymer/BSA complexes, among which the G5-His 80 Cu/BSA complex was the most efficient one (Fig. 3e and f). Negligible Gal8 recruitment was observed in the cells treated with G5-His 80/BSA or G5/BSA complexes. The dendrimer and histidine are widely reported to disturb the endosome by the proposed "proton sponge effect";[43,44] however, the endosome disruption extent is not only affected by the carrier properties but also by the endocytosis level of the complexes.[45] The relatively low cellular uptake of G5-His 80 may contribute to limited endosomal escape. It is worth noting that although the cellular uptake of G5-His 80 Cu was comparable to that of G5-His 80 Ni and lower than that of G5-His 80 Zn, G5-His 80 Cu/BSA exhibited the highest endosomal escape efficacy, indicating the beneficial effect of Cu^{2+} on facilitating the endosomal escape of the functional polymer. The endosomal disruption of G5-His 80 Cu/BSA was time-dependent and was saturated after 4 h incubation (Fig. 3g and S9†). After that, the cargo proteins were released from the complexes in the cytosol triggered by polyanions, proteins, and GSH (Fig. 3h). G5-His 80 Cu exhibited higher efficacy in protein release among the coordinative polymers, which may account for its superior cytosolic protein delivery efficacy.

3.4. Effects of the Cu^{2+} content and histidine grafting ratio on intracellular protein delivery

We further investigated the influence of metal ion contents and histidine grafting ratios on the intracellular protein delivery. As shown in Fig. 4a and Fig. S10,† the EGFP delivery efficiency of Cu^{2+}-coordinated G5-His 80 was significantly improved when the Cu^{2+} to His molar ratio was increased from 0.5 : 1 to 1 : 1; however, the efficacy was decreased when the molar ratio reached 2 : 1. In addition, excessive Cu^{2+} in the delivery system also led to cytotoxicity in the treated cells (Fig. 4c). Similarly, the protein delivery efficiency of Cu^{2+}-co-

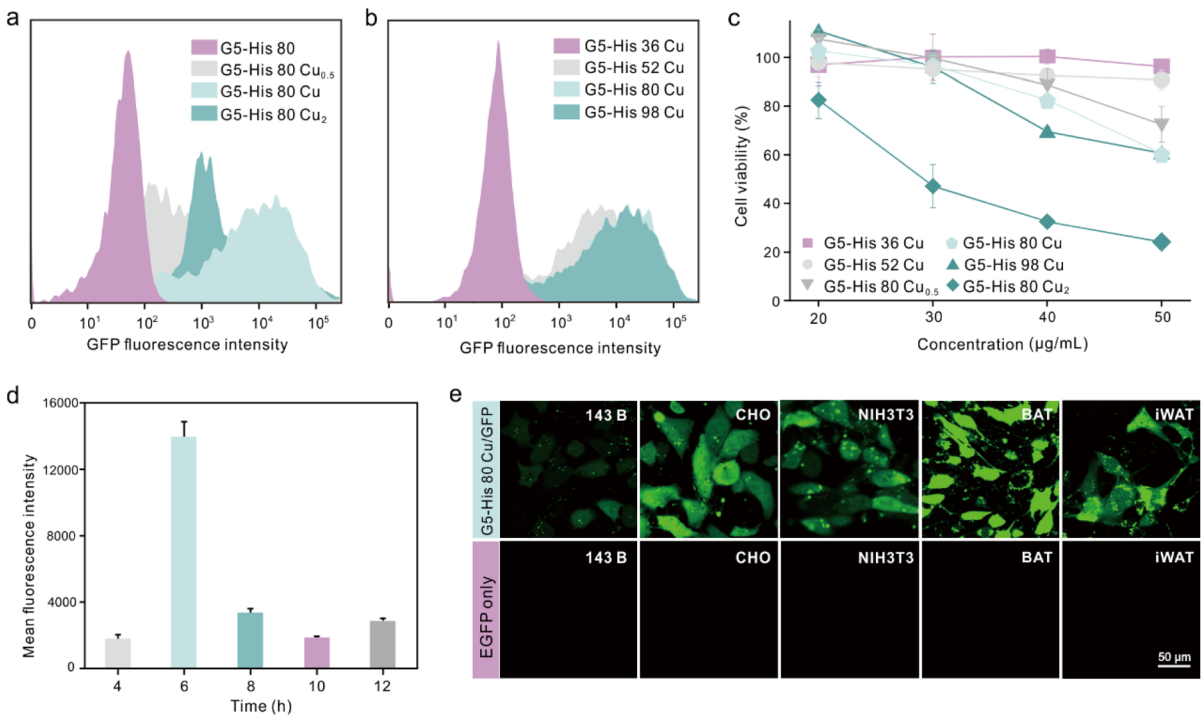

Fig. 4 Cu-coordinated polymers for intracellular protein delivery. (a) EGFP delivery efficacy of the Cu^{2+}-coordinated polymer at different Cu^{2+} to His molar ratios. (b) Flow cytometry analysis of HeLa cells after 6-hour treatment of the complexes. The concentrations of G5-His 36 Cu, G5-His 52 Cu, G5-His 80, G5-His 80 Cu, and G5-His 80 $Cu_{0.5}$ were 40 μg mL^{-1}, and the concentrations of EGFP, G5-His 80 Cu_2, and G5-His 98 Cu were 25 μg mL^{-1}, 20 μg mL^{-1}, and 30 μg mL^{-1}, respectively. (c) Viability of HeLa cells treated with the Cu-coordinated polymers for 24 h at different polymer concentrations. (d) Mean fluorescence intensity of HeLa cells treated with G5-His 80 Cu/EGFP complexes at different times. (e) EGFP delivery efficacy of G5-His 80 Cu on 143B, CHO, NIH3T3, BAT, and iWAT cells. The concentrations of G5-His 80 Cu and EGFP were 40 μg mL^{-1} and 25 μg mL^{-1}, respectively.

ordinated polymers increased with the increasing histidine grafting ratios (Fig. S11†), and G5-His 80 Cu exhibited the highest efficacy (Fig. 4b and S10†). A further increase in histidine modification had no beneficial effect on protein delivery but induced more obvious toxicity in the treated cells (Fig. 4c). Time-dependent delivery experiments showed that HeLa cells treated with G5-His 80 Cu/EGFP complexes for 6 h exhibited the highest protein delivery efficiency (Fig. 4d), and further incubation resulted in a decreased fluorescence intensity owing to the degradation of cargo proteins in the cells. Besides HeLa cells, G5-His 80 Cu showed efficient cytosolic protein delivery efficacy towards various cell lines including human osteosarcoma cells (143B), Chinese hamster ovary cells (CHO), mouse embryo fibroblast cells (NIH3T3), mouse inguinal white adipocyte cells (iWAT) and brown adipose tissue cells (BAT) (Fig. 4e).

3.5. Intracellular β-Gal delivery by coordinative polymers

Finally, we investigated whether the bioactivity of cargo proteins could be maintained after intracellular delivery. β-Gal is a 430 kDa negatively charged membrane-impermeable protein. It can hydrolyze substrate X-gal into galactose and an insoluble blue dye, which can be utilized to visualize the activity of the delivered β-Gal in the cytosol. β-Gal can also hydrolyze the substrate *O*-nitrophenyl-β-D-galactopyranoside (OPNG) into galactose and a yellow-colored *o*-nitrophenol, and the bioactivity of β-Gal can be quantitively valued by measuring the absorbance of the produced *o*-nitrophenol at 420 nm. After being treated with the polymer/β-Gal complexes for 6 hours, HeLa cells were added to X-gal and OPNG, respectively, to evaluate the bioactivity of the internalized β-Gal. As shown in Fig. 5a and b, the cells treated with G5-His 80 Ni/β-Gal and G5-His 80 Zn/β-Gal were observed to have an obvious dark blue color, and more than 65% of β-Gal activities were maintained during the delivery process, which were comparable to the commercial protein delivery reagent TransEx and significantly higher than PULSin. Negligible β-Gal activity was detected in the cells treated with G5-His 80/β-Gal complexes or β-Gal alone. It is worth noting that although G5-His 80 Cu showed the highest efficacy in delivering RB labelled β-Gal (β-Gal-RB) into HeLa cells (Fig. 5c), only 50% of enzymatic bioactivity was recovered in the treated cells, which was lower than that treated with G5-His 80 Ni/

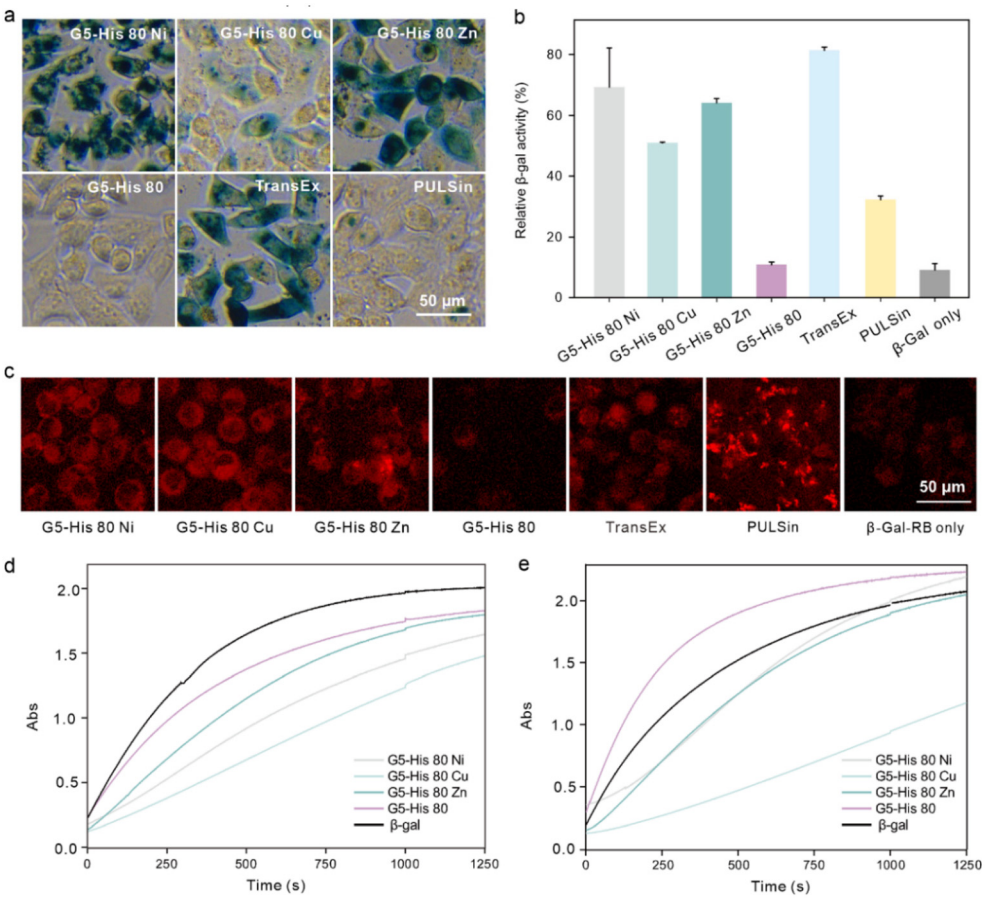

Fig. 5 Intracellular β-Gal delivery by the coordinative polymers. β-Gal activities of HeLa cells treated with the polymer/β-Gal complexes were measured by X-Gal staining (a) and quantitatively analysed using OPNG as the substrate (b). (c) β-Gal-RB delivery efficacy of the coordinative polymers on HeLa cells for 6 h. The concentrations of the polymers, β-Gal and β-Gal-RB were 40 μg mL^{-1}, 25 μg mL^{-1}, and 25 μg mL^{-1}, respectively. (d) Absorbance of β-Gal and polymer/β-Gal complexes after the addition of OPNG for 0–1250 s. (e) Absorbance of β-Gal and polymer/β-Gal complexes in the presence of cytoplasm mimic buffer and added to OPNG for 0–1250 s. The weight ratio of the polymers to β-Gal was 1.6 : 1.

β-Gal and G5-His 80 Zn/β-Gal complexes. To figure out the reasons behind this phenomenon, we tested the β-Gal activity of the polymer/protein complexes *in vitro*. As shown in Fig. 5d, the bioactivities of β-Gal obviously decreased after complexation with G5-His 80 Cu and G5-His 80 Ni, while those slightly decreased in the G5-His 80 Zn and G5-His 80 complexes. The addition of cytoplasm mimic buffer fully recovered the β-Gal activity in the G5-His 80/β-Gal complex due to efficient protein release, and those in G5-His 80 Ni/β-Gal and G5-His 80 Zn/β-Gal complexes were partly recovered. In comparison, the enzymatic activity of G5-His 80 Cu/β-Gal was barely recovered in the presence of cytoplasm mimic buffer, which should account for the relatively lower β-Gal bioactivity in the cells treated with the G5-His 80 Cu/β-Gal complex. Cu^{2+} is considered a "borderline acid" which coordinates favorably with "borderline bases" and "soft bases", such as imidazole, indolyl, and thiol groups of histidine, tryptophan and cysteine, respectively.[35] β-Gal with more tryptophan and histidine moieties than the EGFP exhibited much higher binding affinity with Cu^{2+}, while the high retention of Cu^{2+} on β-Gal in turn led to decreased enzyme bioactivity. Therefore, it might be necessary to adjust the types of metal ions to achieve optimal delivery for different kinds of proteins.

4. Conclusion

In summary, we designed a series of coordinative polymers by modifying histidine ligands on a G5 PAMAM dendrimer and further coordinating them with Cu^{2+}, Ni^{2+}, and Zn^{2+} for intracellular protein delivery. The coordination of metal ions effectively improved the protein delivery efficacy of the histidine-modified dendrimer owing to the beneficial effects of the metal ions in protein binding, complex stability, endocytosis, and endosomal escape. The polymer coordinated with Zn^{2+} ions showed the highest cell internalization and that with Cu^{2+} exhibited the most efficient endosomal escape. This study proves that metal ion/histidine chelate modification can be used as an effective strategy to improve the intracellular protein delivery capability of cationic polymers, which provides new insight into the rational design of protein delivery vehicles.

Conflicts of interest

There are no conflicts to declare.

Acknowledgements

We appreciate the support from the National Natural Science Foundation of China (22005101 and 22135002), the Basic Research Program of Science and Technology Commission of Shanghai Municipality (grant no. 21JC1401800), and the China Postdoctoral Science Foundation (2020M672609).

References

1 S. Mitragotri, P. A. Burke and R. Langer, Overcoming the challenges in administering biopharmaceuticals: formulation and delivery strategies, *Nat. Rev. Drug Discovery*, 2014, **13**(9), 655–672.
2 J. M. Horn and A. C. Obermeyer, Genetic and covalent protein modification strategies to facilitate intracellular delivery, *Biomacromolecules*, 2021, **22**(12), 4883–4904.
3 L. Urquhart, Top companies and drugs by sales in 2021, *Nat. Rev. Drug Discovery*, 2022, **21**(4), 251.
4 R. Goswami, T. Jeon, H. Nagaraj, S. Zhai and V. M. Rotello, Accessing intracellular targets through nanocarrier-mediated cytosolic protein delivery, *Trends Pharmacol. Sci.*, 2020, **41**(10), 743–754.
5 W. He, X. Xing, X. Wang, D. Wu, W. Wu, J. Guo and S. Mitragotri, Nanocarrier-mediated cytosolic delivery of biopharmaceuticals, *Adv. Funct. Mater.*, 2020, **30**(37), 1910566.
6 F. Scaletti, J. Hardie, Y. Lee, D. C. Luther, M. Ray and V. M. Rotello, Protein delivery into cells using inorganic nanoparticle-protein supramolecular assemblies, *Chem. Soc. Rev.*, 2018, **47**(10), 3421–3432.
7 X. Qin, C. Yu, J. Wei, L. Li, C. Zhang, Q. Wu, J. Liu, S. Q. Yao and W. Huang, Rational design of nanocarriers for intracellular protein delivery, *Adv. Mater.*, 2019, **31**(46), e1902791.
8 S. Banskota, A. Raguram, S. Suh, S. W. Du, J. R. Davis, E. H. Choi, X. Wang, S. C. Nielsen, G. A. Newby, P. B. Randolph, M. J. Osborn, K. Musunuru, K. Palczewski and D. R. Liu, Engineered virus-like particles for efficient in vivo delivery of therapeutic proteins, *Cell*, 2022, **185**(2), 250–265.
9 Y. Cheng, Design of polymers for intracellular protein and peptide delivery, *Chin. J. Chem.*, 2021, **39**(6), 1443–1449.
10 J. Lv, Q. Fan, H. Wang and Y. Cheng, Polymers for cytosolic protein delivery, *Biomaterials*, 2019, **218**, 119358.
11 S. Zhang, J. Lv, P. Gao, Q. Feng, H. Wang and Y. Cheng, A pH-Responsive Phase-Transition Polymer with High Serum Stability in Cytosolic Protein Delivery, *Nano Lett.*, 2021, **21**(18), 7855–7861.
12 D. C. González-Toro and S. Thayumanavan, Advances in polymer and polymeric nanostructures for protein conjugation, *Eur. Polym. J.*, 2013, **49**(10), 2906–2918.
13 J. Fu, C. Yu, L. Li and S. Q. Yao, Intracellular delivery of functional proteins and native drugs by cell-penetrating poly(disulfide)s, *J. Am. Chem. Soc.*, 2015, **137**(37), 12153–12160.
14 Y. Lee, T. Ishii, H. Cabral, H. J. Kim, J. Seo, N. Nishiyama, H. Oshima, K. Osada and K. Kataoka, Charge-conversional polyionic complex micelles-efficient nanocarriers for protein delivery into cytoplasm, *Angew. Chem., Int. Ed.*, 2009, **48**(29), 5309–5312.
15 Y. Lee, D. C. Luther, R. Goswami, T. Jeon, V. Clark, J. Elia, S. Gopalakrishnan and V. M. Rotello, Direct cytosolic delivery of proteins through coengineering of proteins and poly-

meric delivery vehicles, *J. Am. Chem. Soc.*, 2020, **142**(9), 4349–4355.
16 E. Bartolami, D. Basagiannis, L. Zong, R. Martinent, Y. Okamoto, Q. Laurent, T. R. Ward, M. Gonzalez Gaitan, N. Sakai and S. Matile, Diselenolane-mediated cellular uptake: efficient cytosolic delivery of probes, peptides, proteins, artificial metalloenzymes and protein-coated quantum dots, *Chemistry*, 2019, **25**(16), 4047–4051.
17 H. Chang, J. Lv, X. Gao, X. Wang, H. Wang, H. Chen, X. He, L. Li and Y. Cheng, Rational design of a polymer with robust efficacy for intracellular protein and peptide delivery, *Nano Lett.*, 2017, **17**(3), 1678–1684.
18 N. D. Posey and G. N. Tew, Associative and dissociative processes in non-covalent polymer-mediated intracellular protein delivery, *Chem. Asian J.*, 2018, **13**(22), 3351–3365.
19 X. Liu, Z. Zhao, F. Wu, Y. Chen and L. Yin, Tailoring hyperbranched poly (β-amino ester) as a robust and universal platform for cytosolic protein delivery, *Adv. Mater.*, 2022, **34**(8), e2108116.
20 C. Liu, T. Wan, H. Wang, S. Zhang, Y. Ping and Y. Cheng, A boronic acid-rich dendrimer with robust and unprecedented efficiency for cytosolic protein delivery and crispr-cas9 gene editing, *Sci. Adv.*, 2019, **5**(6), eaaw8922.
21 L. Ren, J. Lv, H. Wang and Y. Cheng, A coordinative dendrimer achieves excellent efficiency in cytosolic protein and peptide delivery, *Angew. Chem., Int. Ed.*, 2020, **59**(12), 4711–4719.
22 L. Ren, Y. Gao and Y. Cheng, A manganese(II)-based coordinative dendrimer with robust efficiency in intracellular peptide delivery, *Bioact. Mater.*, 2022, **9**, 44–53.
23 Z. Zhang, X. Gao, Y. Li, J. Lv, H. Wang and Y. Cheng, Catechol-based polymers with high efficacy in cytosolic protein delivery, *CCS Chem.*, 2022, DOI: **10.31635/ccschem.022.202202098**.
24 J. Xu, Z. Li, Q. Fan, J. Lv, Y. Li and Y. Cheng, Dynamic polymer amphiphiles for efficient intracellular and in vivo protein delivery, *Adv. Mater.*, 2021, **33**(52), e2104355.
25 W. Xu, F. Luo, Q. Tong, J. Li, W. Miao, Y. Zhang, C. Xu, J. Du and J. Wang, An intracellular pH-actuated polymer for robust cytosolic protein delivery, *CCS Chem.*, 2021, **3**(12), 431–442.
26 Z. Zhang, W. Shen, J. Ling, Y. Yan, J. Hu and Y. Cheng, The fluorination effect of fluoroamphiphiles in cytosolic protein delivery, *Nat. Commun.*, 2018, **9**(1), 1377.
27 Y. Jiang, W. Yang, J. Zhang, F. Meng and Z. Zhong, Protein toxin chaperoned by lrp-1-targeted virus-mimicking vesicles induces high-efficiency glioblastoma therapy in vivo, *Adv. Mater.*, 2018, **30**(30), e1800316.
28 M. P. Stewart, R. Langer and K. F. Jensen, Intracellular delivery by membrane disruption: mechanisms, strategies, and concepts, *Chem. Rev.*, 2018, **118**(16), 7409–7531.
29 M. Luo, H. Wang, Z. Wang, H. Cai, Z. Lu, Y. Li, M. Du, G. Huang, C. Wang, X. Chen, M. R. Porembka, J. Lea, A. E. Frankel, Y. X. Fu, Z. J. Chen and J. Gao, A sting-activating nanovaccine for cancer immunotherapy, *Nat. Nanotechnol.*, 2017, **12**(7), 648–654.
30 J. A. Zuris, D. B. Thompson, Y. Shu, J. P. Guilinger, J. L. Bessen, J. H. Hu, M. L. Maeder, J. K. Joung, Z. Chen and D. R. Liu, Cationic lipid-mediated delivery of proteins enables efficient protein-based genome editing in vitro and in vivo, *Nat. Biotechnol.*, 2015, **33**(1), 73–80.
31 S. Kobayashi, I. Nakase, N. Kawabata, H. Yu, S. Pujals, M. Imanishi, E. Giralt and S. Futaki, Cytosolic targeting of macromolecules using a pH-dependent fusogenic peptide in combination with cationic liposomes, *Bioconjugate Chem.*, 2009, **20**(5), 953–959.
32 D. S. D'Astolfo, R. J. Pagliero, A. Pras, W. R. Karthaus, H. Clevers, V. Prasad, R. J. Lebbink, H. Rehmann and N. Geijsen, Efficient intracellular delivery of native proteins, *Cell*, 2015, **161**(3), 674–690.
33 H. Block, B. Maertens, A. Spriestersbach, N. Brinker, J. Kubicek, R. Fabis, J. Labahn and F. Schäfer, Immobilized-metal affinity chromatography (imac): a review, *Methods Enzymol.*, 2009, **463**, 439–473.
34 V. Postupalenko, D. Desplancq, I. Orlov, Y. Arntz, D. Spehner, Y. Mely, B. P. Klaholz, P. Schultz, E. Weiss and G. Zuber, Protein delivery system containing a nickel-immobilized polymer for multimerization of affinity-purified his-tagged proteins enhances cytosolic transfer, *Angew. Chem., Int. Ed.*, 2015, **54**(36), 10583–10586.
35 E. K. Ueda, P. W. Gout and L. Morganti, Current and prospective applications of metal ion-protein binding, *J. Chromatogr. A*, 2003, **988**(1), 1–23.
36 A. K. Varkouhi, M. Scholte, G. Storm and H. J. Haisma, Endosomal escape pathways for delivery of biologicals, *J. Controlled Release*, 2011, **151**(3), 220–228.
37 A. Sorkin and M. von Zastrow, Signal transduction and endocytosis: close encounters of many kinds, *Nat. Rev. Mol. Cell Biol.*, 2002, **3**(8), 600–614.
38 X. Zhu, R. Tang, S. Wang, X. Chen, J. Hu, C. Lei, Y. Huang, H. Wang, Z. Nie and S. Yao, Protein@inorganic nanodumpling system for high-loading protein delivery with activatable fluorescence and magnetic resonance bimodal imaging capabilities, *ACS Nano*, 2020, **14**(2), 2172–2182.
39 J. Lv, B. He, J. Yu, Y. Wang, C. Wang, S. Zhang, H. Wang, J. Hu, Q. Zhang and Y. Cheng, Fluoropolymers for intracellular and in vivo protein delivery, *Biomaterials*, 2018, **182**, 167–175.
40 J. Lv, H. Wang, G. Rong and Y. Cheng, Fluorination Promotes the Cytosolic Delivery of Genes, Proteins, and Peptides, *Acc. Chem. Res.*, 2022, **55**(5), 722–733.
41 G. Rong, C. Wang, L. Chen, Y. Yan and Y. Cheng, Fluoroalkylation promotes cytosolic peptide delivery, *Sci. Adv.*, 2020, **6**(33), eaaz1774.
42 T. L. Thurston, M. P. Wandel, N. von Muhlinen, A. Foeglein and F. Randow, Galectin 8 targets damaged vesicles for autophagy to defend cells against bacterial invasion, *Nature*, 2012, **482**(7385), 414–418.
43 Y. Wen, Z. Guo, Z. Du, R. Fang, H. Wu, X. Zeng, C. Wang, M. Feng and S. Pan, Serum tolerance and endosomal escape capacity of histidine-modified pdna-loaded com-

plexes based on polyamidoamine dendrimer derivatives, *Biomaterials*, 2012, **33**(32), 8111–8121.

44 J. Yang, Q. Zhang, H. Chang and Y. Cheng, Surface-engineered dendrimers in gene delivery, *Chem. Rev.*, 2015, **115**(11), 5274–5300.

45 K. V. Kilchrist, S. C. Dimobi, M. A. Jackson, B. C. Evans, T. A. Werfel, E. A. Dailing, S. K. Bedingfield, I. B. Kelly and C. L. Duvall, Gal8 visualization of endosome disruption predicts carrier-mediated biologic drug intracellular bioavailability, *ACS Nano*, 2019, **13**(2), 1136–1152.